Chapter 22
Modelling the Overflows Across the Greenland–Scotland Ridge

Johann H. Jungclaus[1], Andreas Macrander[2], and Rolf H. Käse[3,4]

22.1 Introduction

The Atlantic Meridional Overturning Circulation (AMOC) is part of a global redistribution system in the ocean that carries vast amounts of mass, heat, and freshwater. Within the AMOC, water mass transformations in the Nordic Seas (NS) and the overflows across the Greenland–Scotland Ridge (GSR) contribute significantly to the overturning mass transport. The deep NS are separated by the GSR from direct exchange with the subpolar North Atlantic. Two deeper passages, Denmark Strait (DS, sill depth 630 m) and Faroe Bank Channel (FBC, sill depth 840 m), constrain the deep outflow. The outflow transports are assumed to be governed by hydraulic control (Whitehead 1989, 1998). According to the circulation scheme by Dickson and Brown (1994), there is an overflow of 2.9 Sv (1 Sv = 1 Sverdrup = 10^6 m^3 s^{-1}) through DS, 1.7 Sv through FBC and another 1 Sv from flow across the Iceland–Faroe Ridge (IFR). To the south of the GSR, the overflows sink to depth and then spread along the topography, eventually merging to form a deep boundary current in the western Irminger Sea. During the descent, the dense bottom water flow doubles its volume by entrainment of ambient waters (e.g. Price and Baringer 1994) so that there is a deep water transport of 13.3 Sv once the boundary current reaches Cape Farvel (Dickson and Brown 1994). Thus the overflows and the overflow-related part of the AMOC account for more than 70% of the maximum total overturning, which is estimated from observations to be about 18 Sv (e.g. Macdonald 1998).

Climate model studies (e.g. Schmittner et al. 2005) indicate a considerable decrease of the AMOC and a reduction of the heat transport under global warming

[1]Max Planck Institute for Meteorology, Bundesstrasse 53, 20146 Hamburg, Germany, e-mail: johann.jungclaus@zmaw.de

[2]Alfred Wegener Institute for Polar and Marine Research, Bussestrasse 24, 27570 Bremerhaven, Germany

[3]Institut für Meereskunde, Universität Hamburg, Bundesstrasse 53, 20146 Hamburg, Germany

[4]IfM-Geomar, Leibniz Institute for Marine Research, Düsternbrooker Weg 20, 24105 Kiel, Germany

R.R. Dickson et al. (eds.), *Arctic–Subarctic Ocean Fluxes*, 527–549

conditions, mainly due to increasing static stability of the upper ocean in high latitudes. Given the role of the overflow-related contribution to the present-day AMOC, it is of importance to elucidate the underlying processes in the present and future climate, and their proper representation in numerical models. This holds in particular for large-scale, coarse-resolution climate models. Summarizing the state-of-the-art at the time of the release of the International Panel of Climate Change (IPCC) third assessment report, Stocker et al. (2001) conclude that the "uncertainties in the representation of the flow across the GSR limit the ability of models to simulate situations that involve a rapid change in the THC". In relatively coarse resolution ocean general circulation models (OGCMs), the overflows across the GSR and the AMOC have been found to be sensitive to the geometry of the throughflow channels. At grid sizes of the order of 100 km, changes in the representation of the topography may result in considerable changes of the overflow transports and its water mass composition. For example, Roberts and Wood (1997) found a 50% change in heat flux at the GSR latitude when a single grid box was modified. Moreover, some OGCMs feature quite unrealistic depth and width of the channels (e.g. Schweckendiek and Willebrand 2005).

The throughflow transports are determined by hydraulic control and it is not clear which numerical resolution is required to properly simulate the partly nonlinear processes involved. If the grid size is too large and the simulated velocities and Froude numbers are too small, the information exchange between the dense layers north and south of the GSR, which under appropriate physics is only in one direction, occurs in both directions.

The fate of the overflow waters once they have passed the sill depends on the amount of mixing they experience downstream. Observations indicate that there is an entrainment of the order of 100% of the original volume transport and that the mixing often occurs over steep slopes on very small horizontal distances (e.g. Baringer and Price 1997). In recent years, several attempts have been made (see Section 3.1) to parameterize the downslope flow and the entrainment in GCMs.

Here, we review first the development in theory and process modelling touching on hydraulics and dense gravity currents. Then, as a major part of the paper, we describe the representation of the overflow in high-resolution regional models and in a coarse-resolution state-of-the-art climate model. The sensitivity of the overflow to climate variations on interannual to decadal variations and to anthropogenic global warming is discussed.

22.2 Hydraulics of Sill and Strait Flow

Analytical theories of flows through passages and across sills (Gill 1977; Whitehead 1989; Killworth and McDonald 1993; Whitehead 1998) are important concepts to investigate transport limits of the outflow. Considerable progress has been made in the last decade to understand the nature of overflows in theory and by analysis of new observations. We mention here the special volume on "The Physical Oceanography

of Sea Straits" (Pratt and Smeed 2004) that addresses topics, such as hydraulic control, mixing and friction as well as far-field effects and time dependence. In view of the importance of overflows for the stability of the AMOC, increasing interest was laid on the applicability of a 'weir' formula that would allow one to characterize the strength of the outflow by a relationship between the total outflow Q and a 'proxy' variable that could be measured without much instrumental efforts. The rationale for this approach is based on the fact that in hydraulically controlled flows, velocity and interface height are not independent, so that the determination of one would allow the calculation of the other. Unfortunately, analytical solutions are restricted to cases with simple bathymetry-like rectangular or parabolic cross-sections and certain assumptions on the upstream potential vorticity. An often-used prediction for a rotating rectangular channel (Whitehead 1989) is

$$Q = g' \frac{h_u^2}{2\mathrm{f}}; \quad L > \sqrt{\left(2g' \frac{h_u}{f^2}\right)}; \tag{22.1}$$

and

$$Q = \left(\frac{2}{3}\right)^{\frac{3}{2}} L\sqrt{(g')}\left[h_u - \frac{f^2 L^2}{8\mathrm{g}'}\right]^{\left(\frac{3}{2}\right)}; \quad L \leq \sqrt{\left(2g' \frac{h_u}{f^2}\right)} \tag{22.2}$$

with Coriolis parameter f, width of the channel L, the reduced gravity based on the density difference between an upstream and downstream reference profile g', and the height of the bifurcation depth h_u (Fig. 22.1). Whitehead (1998) investigated a large number of ocean gateways and found that his hydraulic predictions ranged from a factor 1 to 2.7 against volume flux estimates. For the passages of interest here, the Denmark Strait and the Faroe Bank Channel, the factor was 1.3 and 1.6, respectively.

Nikolopoulos et al. (2003) showed that the maximum volume flux for Denmark Strait was in much better agreement with observations if a more realistic geometry was included. A parabolic profile is also suggested to be a better approximation for the Faroe Bank Channel (Borenäs and Lundberg 1988), which results in an estimate for the volume flux

$$Q = \frac{h_u^2}{2+r}\sqrt{\left(\frac{3\mathrm{f}^2}{2\mathrm{r}}\right)}; \quad r = a\frac{f^2}{g'}$$

with the coefficient a of the parabolic depth profile.

Helfrich and Pratt (2003) revisited Gill's (1977) theory for rotating hydraulic sill flow, which assumes semigeostrophic flow of uniform potential vorticity through a

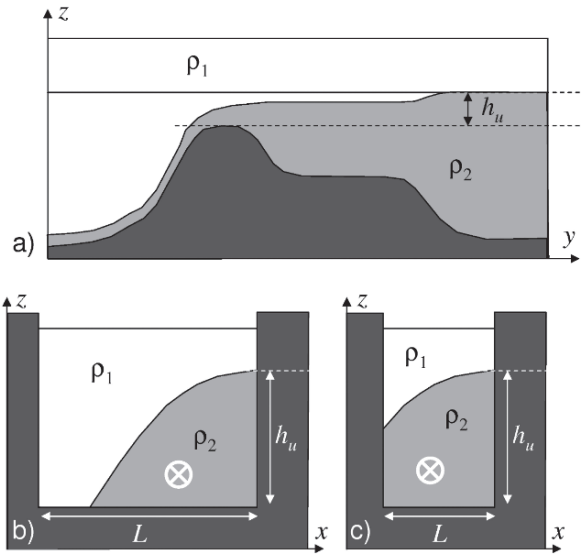

Fig. 22.1 Schematic of the hydraulic flow over a sill: along-channel view (a), and cross-channel view for (b) wide (Eq. 22.1) and (c) narrow (Eq. 22.2) upstream channel configuration, respectively

rectangular channel, and compared it with results from a reduced-gravity shallow water model for a combined basin and sill configuration. The coupled basin-strait system was shown to "select" an average overflow potential vorticity corresponding to Gill's solution. Another interesting finding is that robust estimates of the sill transports from upstream conditions can only be obtained if these conditions are taken from the strait entrance, not from the basin interior.

22.3 Modelling the Outflow Plume Downstream of the Sill

The numerical modelling of gravity currents was initiated by the stream-tube model of Smith (1975). This model, as well as refined versions, which take into account, for example, variable topography (Price and Baringer 1994), considers a stationary, laterally integrated stream-tube with variable cross-sectional area. Several applications showed that such a model is able to reproduce the pathway and the along-pathway evolution of water mass properties (e.g. Baringer and Price 1997). Girton and Sanford (2003) used observed quantities and were able to quantify the balance of terms that govern the descent of the Denmark Strait overflow plume. They found a balance between the terms describing loss of potential energy and bottom friction. It is interesting to note that no entrainment stress at the interface was taken into

account. In view of the strong mixing due to the presence of eddies (Bruce 1995), the expected descent pathway agrees surprisingly well with the observations (see Fig. 2 of Girton and Sanford 2003). This rate differs markedly from other models such as that of Killworth (2001) who claims a constant descent rate of 1/400.

The stream-tube model does not give any information about the spatial structure of the plume. Therefore, Jungclaus and Backhaus (1994) developed a two-dimensional transient reduced-gravity model that resolves the horizontal structure of the plume and is able to simulate the splitting and merging of the plume. Substantial progress in the understanding of the dynamics of the overflow plume was achieved after including the vertical dimension in high-resolution process studies with three-dimensional general circulation models (GCM). Using a sigma-coordinate model, Jiang and Garwood (1996) were able to simulate the three-dimensional evolution of an overflow plume on an idealized continental slope. They showed that the plume breaks apart into a chain of eddies and that these eddies exhibit a pronounced surface expression, so that the overflow may be tracked by satellite imagery. The destabilization of the gravity current has been further investigated in the numerical studies of Jungclaus et al. (2001), Shi et al. (2001), and Ezer (2006). Using the MIT z-coordinate GCM Riemenschneider and Legg (2007) have investigated the dependence of the representation of the FBC overflow on grid resolution and mixing parameterisations. They show that the structure and properties of the overflow plume is comparable with observations at the highest resolution of 2 km where the Rossby radius is clearly resolved and the ratio between horizontal and vertical resolution allows for an adequate representation of the fluxes (see below). The numerical mixing in the model is found to be most sensitive to changes in horizontal resolution, and to a lesser extent on vertical resolution and vertical viscosity.

22.4 Parameterization of Dense Outflow and Bottom Boundary Layer Processes in Large-Scale Ocean Models

The ultimate goal of these idealized model exercises is to use the knowledge obtained from process studies to develop improved parameterizations for large-scale models. The model intercomparison study carried out in the Dynamics of North Atlantic Models (DYNAMO) project (Willebrand et al. 2001) showed that the proper representation of the mixing depends much on the choice of the vertical coordinate. Most climate OGCMs are formulated on depth coordinates and obtain far too much mixing for dense overflows at a sill. Due to the staircase-like representation of the bottom topography, downslope flow is simulated as a succession of horizontal advection and a (convective) overturning. Models with terrain-following vertical (sigma or s) coordinates perform better but often require a substantial smoothing of the topography in order to avoid spurious effects in the horizontal pressure gradient formulation. Isopycnic models have been shown to reproduce realistic dense outflow plumes once diapycnic mixing is properly parameterized (Hallberg 2000; Xu et al. 2006).

The correct simulation of the overflow pathways downstream of the sill and the entrainment of ambient waters into the plume is therefore challenging for coarse resolution *z*-coordinate models. Winton et al. (1998) estimated that a horizontal resolution of $\Delta x = \Delta z/\alpha$ is required, where α is the bottom slope, and that the bottom boundary layer should be resolved by several points.

In coarse-resolution models, more realistic down slope flow and water mass transformation have been achieved by parameterizing the turbulent bottom boundary layer (BBL). There are two different approaches to achieve this goal. One relatively simple 'plumbing' approach is to reduce the spurious mixing by connecting grid cells above and below a topographic step (Beckmann and Döscher 1997; Campin and Goosse 1999; Marsland et al. 2003). In the latter scheme for example (see Marsland et al. 2003, their Fig. 1), the dense water flow is redirected into a deeper level (but not necessarily the bottom level, as in Beckmann and Döscher 1997) of an adjacent grid. The target depth is determined by the stratification of the receiving grid cell, similar to the approach by Campin and Goosse (1999). On the other hand, Killworth and Edwards (1999) and Song and Chao (2000) couple a full two-dimensional bottom boundary layer model to a GCM. This allows for a more physically based approach to determine both detrainment and entrainment. For example, Killworth and Edwards (1999) employ a frictional bottom boundary layer to determine the mixing rates. Whereas the 'plumbing' schemes are used in a number of large-scale models, the BBL sub-modules have not found their way into climate GCMs, to our knowledge. Currently, there is a coordinated project founded by the US National Science Foundation to evaluate and improve overflow parameterisations. The Climate Process Team on Gravity Currents and Entrainment (http://cpt-gce.org/) aims to combine observational programmes and numerical modelling reaching from extremely high-resolution non-hydrostatic models (Özgökmem et al. 2006) to GCM analyses (Legg et al. 2006).

Another approach to parameterize the overflow in models with low resolution is to determine the transport directly from hydraulic relations (Kösters et al. 2005). Their application of a hydraulic transport parameterization to a coarse resolution ocean model gave a considerable increase in both the AMOC and the meridional heat transport that resulted in 1 K warmer air temperatures over Europe compared to the standard model set-up.

22.5 Regional Models of the Exchange Flow Across the GSR

High-resolution limited-area models with realistic bottom topography allow one to compare the results with theoretical estimates, such as upper bounds on hydraulic transports. In a numerical process model, Käse and Oschlies (2000) calculated the exchange between two basins that are connected by a strait with bathymetry mimicking the Denmark Strait. The application of a bottom-following vertical coordinate and a horizontal resolution of about 4 km allowed for a quite realistic representation of bottom boundary layer processes and eddies. Käse and Oschlies filled the upstream

basin from the northern boundary, while permitting the lighter water to leave via the northern boundary to obtain a net zero mass flux. Käse and Oschlies (2000) found that the transport is topographically controlled and the predictions of Whitehead (1998) and Killworth and McDonald (1993) are consistent with the model results. The dense sill flow increased according to the increasing northern basin interface height, which became stationary when the prescribed inflow equaled about 60% of the Whitehead (Eq. 22.1) maximum flux. Stern (2004) offered an alternative explanation for this factor independent of hydraulic arguments. He investigated the maximum geostrophic flow through a parabolic bottom shape and found a theoretical factor of 9/16 of the Whitehead value. It has to be noted that the height scale h_u in Stern's formulation is taken at the right hand side wall of the parabolic channel.

A recent re-assessment of the Käse and Oschlies (2000) simulations revealed that the plume thickness and the sea surface elevation (SSH) are highly correlated. Figure 22.2 shows the correlation between these two quantities near the sill. The narrow flow path is related to a depression in SSH. The overflow path and its variability might therefore be observed by altimetry. This aspect was investigated in more detail by Köhl et al. (2007). They use a high-resolution (0.1°) regional model including the entire GSR that is embedded in the 1° global ECCO model (Stammer et al. 2002) and that is forced with NCEP reanalysis data for the 1990s. They found high correlations between interface height and SSH in the strait and around Iceland (their Fig. 10, and see below) and were able to reconstruct (simulated) overflow transports by regression to SSH. In general, the theories of Whitehead (1989) and Gill (1977) that describe the steady maximum transport over a sill were found to be

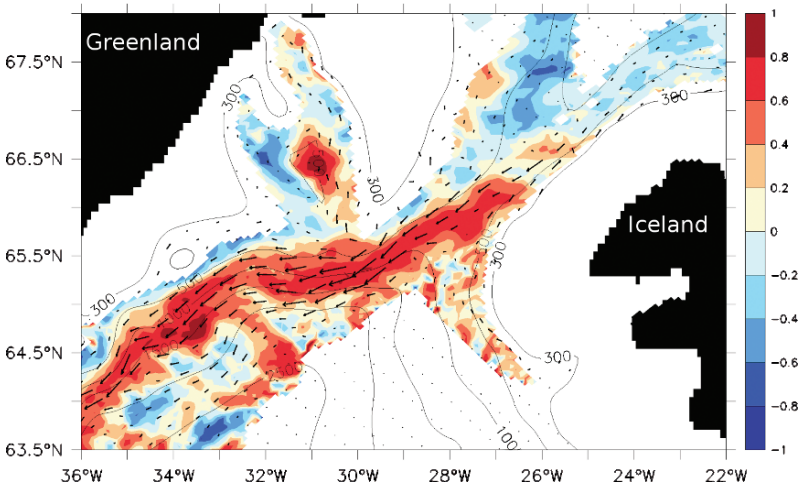

Fig. 22.2 Point-to-point correlations between the interface depth and the SSH in the Käse and Oschlies (2000) model. Note that positive correlations indicate negative SSH anomalies overlying positive thickness (negative interface depth) anomalies

consistent with the simulated mean transport and even with its variations as long as the timescale is much longer than the synoptic scale. Thus transport variations can be inferred from measuring the upstream interface height in the vicinity of the strait entrance, and possibly, altimetry. An attempt to apply the reconstruction of overflow transport by regression with SSH from observed data revealed unforeseen difficulties and Köhl et al. (2007) concluded that very high accuracy in the observation is required.

22.6 The Representation of the Overflows in Large-Scale Climate Models

22.6.1 The Mean State: Transports Across the GSR and Water Mass Properties

The simulation of the NS circulation with state-of-the-art ocean models driven by prescribed atmospheric fluxes obtained from reanalysis has recently been reviewed by Drange et al. (2005) and applications to the exchanges between the Nordic Seas and the North Atlantic have been published by Haak et al. (2003), Nilsen et al. (2003), and Zhang et al. (2004). Even though the simulation of the overflows was not the main focus of these papers, the studies showed that present-day OGCM can, given the correct forcing and its variability, quite realistically reproduce the observed exchange processes across the GSR.

Simulating these processes with a coupled atmosphere–ocean model is even more challenging. In climate modelling, one major breakthrough over the last few years has been that most models no longer need flux adjustments to maintain a stable climate. The reason for that improvement may be sought as well in the atmospheric or oceanic GCMs. A consequence is, however, that the (although stable) mean state of the surface climate may differ substantially from observations (e.g. Jungclaus et al. 2006a). As an example of a typical state-of-the-art model, we present results from the Max Planck Institute for Meteorology (MPI-M) climate model that participated in the IPCC Fourth Assessment Report (AR4). The simulations were conducted with the coupled atmosphere–ocean–sea ice general circulation model ECHAM5/MPIOM. The atmospheric part of the model, ECHAM5 (Roeckner et al. 2003), has a horizontal resolution of 1.875° by 1.875° (T63) and 31 vertical levels. The ocean/sea ice part of the model, MPIOM (Marsland et al. 2003), has a 1.5° by 1.5° horizontal resolution on a curvilinear grid with 40 vertical levels. MPIOM uses a curvilinear orthogonal grid and the two grid poles are placed upon Antarctica and Greenland thus avoiding the pole-singularity problem at the North Pole and providing relatively high resolution in the deep-water formation regions of the Labrador Sea and the Greenland Sea (see Jungclaus et al. 2006a, their Fig. 1). Denmark Strait (DS) is located close to the grid pole over Greenland and is resolved by several grid points at 15–25 km resolution (Fig. 22.3). DS sill depth is 600 m. Following the

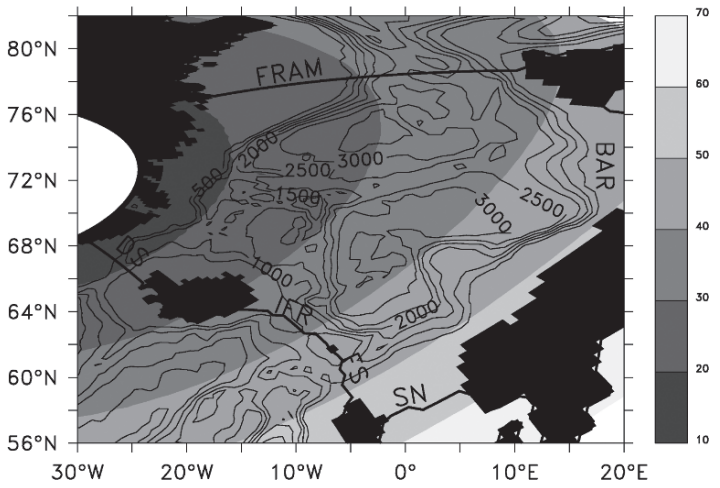

Fig. 22.3 Bottom topography (contours) of the Greenland–Scotland Ridge and Nordic Seas region in the global ocean model MPIOM. Gray shadings (units = km) show the numerical grid size and solid black lines indicate the sections across Denmark Strait (DS), along the Iceland–Faroe Ridge (IFR), the Faroe–Scotland section (FS), the Scotland–Norway section (SN), the Barents Sea opening (BAR), and the section across the Fram Strait (FRAM). Contour interval (ci) for topography = 500 m

Table 22.1 Overview over the exchanges across the GSR. Mean values and standard deviations of mass and heat transports

Section	Total (Sv)	Into NS (Sv)	Out NS (Sv)	$\sigma_\theta > 27.8$ (Sv)	$\sigma_\theta < 27.8$ (Sv)	HTR (TW, total)
DS	−4.7 ± 0.5	1.5 ± 0.16	−6.2 ± 0.6	−3.3 ± 0.5	−1.4 ± 0.3	−5 ± 8
IFR	4.5 ± 0.6	6.4 ± 0.6	−1.8 ± 0.2	0	4.5 ± 0.6	188 ± 25
FS	0.37 ± 0.6	3.9 ± 0.5	−3.5 ± 0.2	−3.0 ± 0.2	3.3 ± 0.6	123 ± 26
SN	0.2 ± 0.05	1.3 ± 0.1	−1.1 ± 0.1	0	0.2 ± 0.05	3 ± 2

Iceland–Scotland Ridge (ISR) to the east, the grid size widens and is about 50 km in the Faroe–Scotland section. The Faroe Bank Channel (FBC) is the deepest outlet with a depth of 890 m. The bottommost section is, however, just resolved by one velocity grid point. At the sill depths, the vertical resolution is 80 m at 600 m depth and 120 m at 900 m depth.

The results shown here stem from a 505-year long control integration under pre-industrial conditions for greenhouse gas concentration. It has been preceded by a multicentury spin-up run that was started from the PHC climatology (Steele et al. 2001). Various aspects of the mean state and internal variability in the ECHAM5/MPI-OM IPCC set-up have been discussed by Jungclaus et al. (2006a), Müller and Roeckner (2006), and Bengtson et al. (2006).

We begin the discussion of the exchanges across the GSR by an account of the mean fluxes in Table 22.1. The $\sigma_\theta = 27.8\,\mathrm{kg\ m^{-3}}$ interface is traditionally taken as

the boundary between the warm inflow and the cold outflow. In the model, there seems to be some recirculation of AW across the IFR. In total, IFR and FS contribute 7.8 Sv (4.5 Sv and 3.3 Sv, respectively) to the warm inflow into the Nordic Seas. Direct measurements by Østerhus et al. (2005) gave 3.8 Sv for each section and an additional 0.8 Sv inflow through DS, where the model simulates 1.4 Sv. The deep outflow in DS of 3.3 Sv is somewhat higher than the often-quoted 2.9 Sv of Ross (1984) and of Dickson and Brown (1994) but compares well with the most recent measurements of 3–3.5 Sv by Macrander et al. (2005). These numbers depend, however, to some extend on the exact location of the section. There is an outflow of 3 Sv dense ($\sigma_\theta > 27.8$) water through FS but profiles of the flows averaged across the sections (c.f. Fig. 22.6c) indicate that the 27.8 criterion is too restrictive for the FS outflow. Hence, FS outflow is taken to be all outflow with density $\sigma_\theta > 27.6$, which increases the mean FS outflow transport to 3.6 Sv. This number is considerably higher than the observed transport estimates of 2 Sv (Saunders 1990; Borenäs and Lundberg 2004). However, since in the model there is no overflow across the IFR (assumed from observations to account for roughly 1 Sv (Dickson and Brown 1994)), the 3.6 Sv represent the total dense outflow through the Iceland–Scotland section. Most likely, the model IFR topography does not resolve small overflow channels and the dense water there is guided by the ridge towards the FS section and escapes through the FBC. In total, the model simulates a mass transport overturning of more than 6 Sv across the GSR. Since no deep water is flowing through the Canadian Archipelago this overturning reflects the water mass transformation in the NS and in the Arctic (not taking any contributions from the Bering Strait into account). From budget considerations the outflow of water $\sigma_\theta > 27.8$ must be balanced by production (flux through the $\sigma_\theta = 27.8$ interface) and the time derivative of the interface height (reservoir changes). Many previous coarse resolution climate models 'closed' the overturning cell with deep convection to the south of the GSR and did not include a proper contribution from the overflows and from water mass transformation to the north of the GSR. In the MPI-M model, 30% of the entire Atlantic overturning of about 22 Sv comes directly from the Nordic Seas. Together with the roughly 100% entrainment that occurs to the south of the sills, the northern branch forms the backbone of the overturning and plays therefore a more pronounced role compared to earlier climate models. Heat transports across the sections add up to 0.31 PW. Decomposition of the heat transport across the entire GSR into depth independent (gyre) and overturning contribution (e.g. Gulev et al. 2003) shows that the heat transport is dominated by the gyre (0.21 PW), but variations in gyre and overturning heat transports are of similar magnitude (standard deviations are about 0.015 PW)). The total heat transport is quite similar to those deduced from observations (e.g. 0.275 PW by Blindheim and Østerhus (2005), and 0.313 PW (Østerhus et al. 2005)).

The model simulated near-surface circulation (not shown) in the transition region between the Atlantic and the Nordic Seas (NS) shows the well-known features of the East Greenland Current (EGC), carrying cold and fresh Arctic water masses to the south, and the three branches of the Atlantic inflow, the Irminger Current to the west of Iceland, the Faroe Current that crosses the GSR near

Iceland, and the slope current along the northwestern European continental slope. To the north of the IFR, the currents move eastward and the North Irminger Current (NIC) and Faroe Current extensions join the slope current to form the Norwegian Atlantic Current. The simulated circulation broadly agrees with available observations (e.g. Jakobsen et al. 2003).

The potential density isosurface $\sigma_\theta = 27.8$ is often used as the boundary between the upper layer and the outflow. In the simulation, the maximum outflow densities exceed $\sigma_\theta = 27.9$ in DS and occasionally 28.0 in the FBC. The mean topography of the $\sigma_\theta = 27.8$ surface is depicted in Fig. 22.4. The interface is deep in the east where Atlantic water masses dominate and shallow in the Greenland Sea and Iceland Sea. Outcropping regions exhibit strong temporal variability over the simulation (not shown). The volume of waters denser than $\sigma_\theta = 27.8$ is maintained by inflow through Fram Strait, convection, diapycnal mixing in the basin, and the outflow through the DS and FS. In the simulation, there is no direct outflow of this water mass across the IFR and only a small amount of water with $\sigma_\theta > 27.7$ crosses the sill from north to south. In the interior NS, the interface height is several hundred meters higher than the sill depths and it is the potential energy stored here that drives the overflows. The transport integrated from the bottom to the $\sigma_\theta = 27.8$ surface gives some indications on the flow paths feeding the overflows (Fig. 22.4). There is inflow of dense waters from Fram Strait, and the cyclonic basin circulation features a pronounced boundary current below the EGC. Approaching DS, the flow splits up into two paths, one that continues on the East Greenland continental shelf and another branch that approaches DS from the northeast. As has been shown by Käse and Oschlies (2000) and Helfrich and Pratt (2003), the eastern branch is

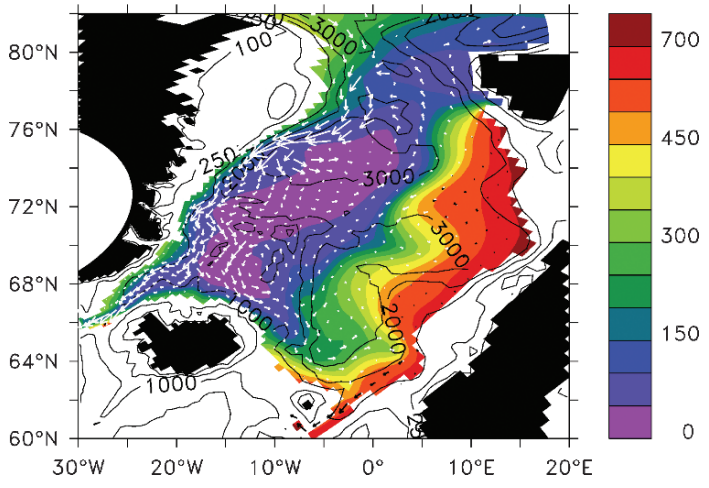

Fig. 22.4 Simulated mean depth (m) of the $\sigma = 27.8\,\mathrm{kg\ m^{-3}}$ isosurface (shading) together with bottom topography (contours) and transports ($\mathrm{m^2\ s^{-1}}$, every other vector shown) integrated from the bottom to the 27.8 surface. For interface depths below 500 m vectors are plotted in black

a consequence of potential vorticity conservation for a flow approaching a sill. This could be a dynamical explanation for the eastern flow path that has recently been described from observations (Jónsson and Valdimarsson 2004). There is eastward flow along the northern slope of the ISR and the FSC/FBC outflow is fed, in part, by these waters.

Sections through the outflow channels DS and FS (Fig. 22.5a and c, respectively; for locations see Fig. 22.3) are given for the simulated along-channel velocities and the potential densities. For DS, the respective fields are also available from a vessel-mounted acoustic doupler current profiler (ADCP) and hydrographic observations (Fig. 22.5b). At the DS sill (Fig. 22.5a), in the upper part of the strait, the western side is dominated by the light and fresh Arctic waters from the EGC separated from the warm Atlantic waters of the NIC. The dense overflow water can be found below 200 m and its density exceeds 27.9 below 400 m. Observations (Fig. 22.5b) indicate densities above 27.8 occupying a large part of the western slope. The thickness of the overflow layer (water denser than 27.8) is roughly 300 m in both observations and simulations. The isopycnal is steeply inclined directly above the deepest part of the channel but the slope changes sign above the western slope. The along-channel velocity has a maximum roughly 100 m above the bottom but the coarse vertical resolution does not allow for a proper representation of a well-mixed boundary layer. The along-channel velocity maximum near the surface is located about 60 km west of the channel axis but the velocity structure is quite barotropic. In the observations there is indication of an eddy but Macrander (2004) confirms that the general flow patterns have been robust for a number of other cruises. A remarkable feature is that the flow is quite barotropic despite of the large density contrasts with the steeply inclined isopycnals. In contrast to DS, the simulated current structure across the Faroe–Shetland channel (Fig. 22.5c) shows the features of a two-layer exchange flow with a zero crossing of the velocity profile at mid-depth. Again, the coarse horizontal and vertical resolution does not allow the detailed simulation of, for example, the velocity profile (Hansen et al. 2001) or the relatively thick, well-mixed boundary layers that are associated with cross-slope Ekman fluxes (Jungclaus and Vanicek 1999). It should be noted, however, that even though the model is able to simulate the density structure quite realistically, it fails to reproduce the water mass properties. The overflow waters are up to 2 K too warm and 0.3 psu too salty (not shown).

As has been discussed in Section 22.4, a proper representation of the sinking and mixing in the overflow plume is quite challenging for GCMs. In MPIOM, a slope convection parameterization was implemented and Marsland et al. (2003) showed that the scheme improved the near bottom water mass characteristics to the south of the GSR even though a vertical grid resolution of 100–300 m at 2,000 m depth does not allow for a 'realistic' vertical structure of the plume. Furthermore, the horizontal resolution is far too coarse to allow horizontal eddies with a radius of about 50–100 km to develop (Jiang and Garwood 1996; Jungclaus et al. 2001). In the coupled simulation presented here, the overflows mix with ambient waters downstream of the sills, but can be traced as a dense bottom current that follows the topographic contours (Fig. 22.6). The Faroese outflow flows along the southern

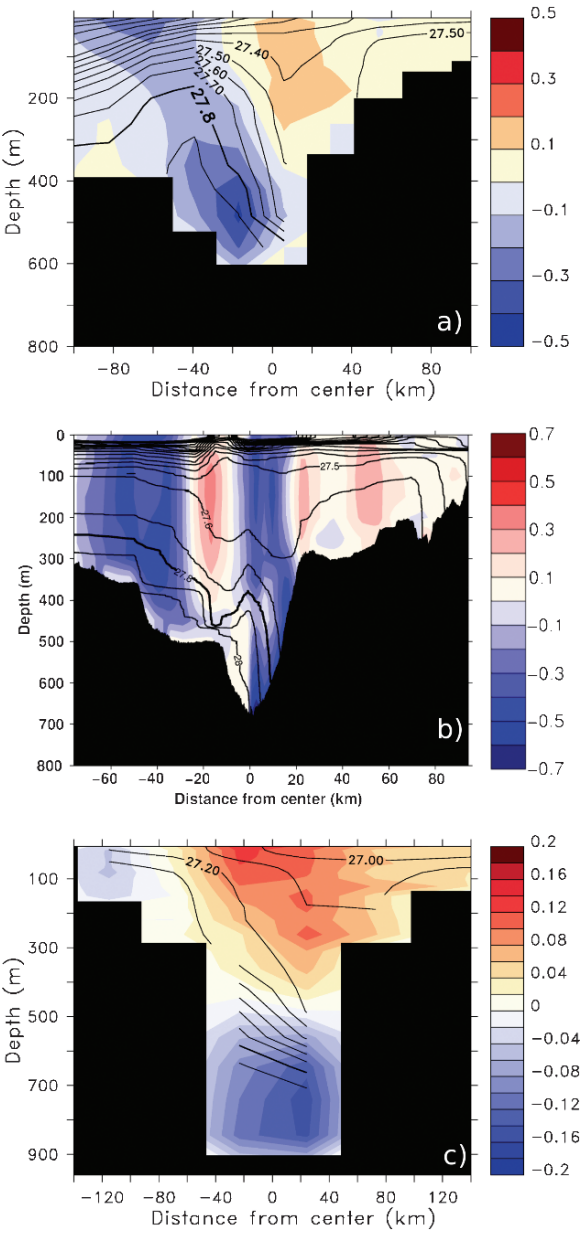

Fig. 22.5 Density (contours) and along-channel velocity (shading in m s^{-1}) sections through the DS and the FS: (**a**) simulated mean DS, (**b**) observed DS, and (**c**) simulated mean FS section. The observed along-channel velocities (**b**) were measured by vessel-mounted ADCP during Poseidon P262 cruise in July 2000 and potential density was derived from hydrographic CTD data. *X*-axis is in kilometers from west to east relative to the channel centre

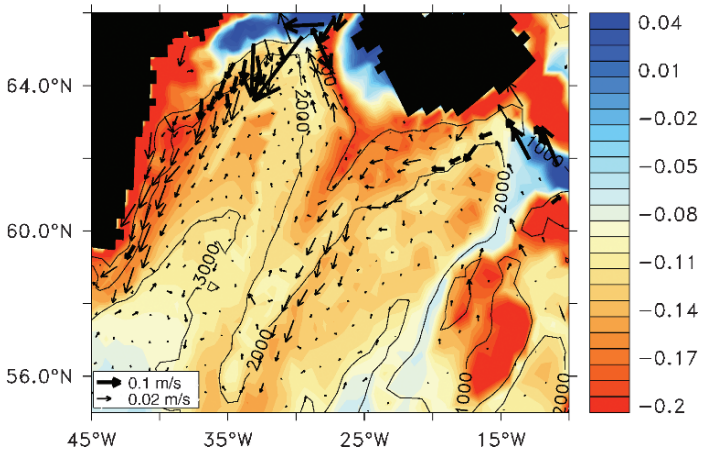

Fig. 22.6 Simulated properties to the south of the GSR: Mean near-bottom velocities (vectors). For clarity, current velocities exceeding 0.05 m s^{-1} are indicated by bold arrows with lengths downscaled by a factor of 3. Mean deviation of the near bottom density (kg m^{-3}) from the respective field from the PHC climatology shaded in the background

edge of the ISR and is then deviated southward by the Reykjanes Ridge. The bottom current occupies a depth range of 1,000–2,500 m. At various depths, the flow enters the Irminger Basin. However, the flow loses intensity and excess density by mixing and there is only weak northward flow along the western edge of the Reykjanes Ridge. The bottom density error is smallest near the exit of the FBC. The DS is characterized as a strong boundary flow along the Greenland continental slope. The bottom density is too high at the upslope edge near the strait, indicating that the flow doesn't sink to the proper depth immediately downstream of the strait. In general, the density deviations at the sills are relatively small but increase with distance, indicating that even with a slope convection parameterization the correct bottom density is hard to achieve. Moreover, as has been mentioned above, the simulated water mass properties in the Nordic Seas are off quite substantially due to too warm and salty Atlantic inflow but probably also due to insufficiencies in the parameterization of vertical mixing and convection. As a result, the overflow waters are also too warm and too salty, even though their density at the sill, owing to compensating effects of temperature and salt, compares relatively well with the observations. This will have effects on the density by ways of the nonlinear equation of state and the differential mixing of heat and salt. Errors in the water mass properties appear to be the major shortcomings in the present simulation. In comparison to earlier models using flux adjustment, the results are probably even worse because much of the (near surface) errors in SST, precipitation, etc. was masked by the corrections. A systematic review of this problem is beyond the scope of this paper and a thorough evaluation of several climate models using different parameterizations is necessary. Progress is also expected from detailed process studies,

such as those currently carried out within the framework of the Climate Process Teams on gravity flows (see Section 22.4).

22.6.2 *Variability of the GSR Exchange and Overflows in the Climate GCM*

While the long-term overturning circulation across the GSR is determined by the production of dense water in the NS and in the Arctic, variations of the overflow transports are determined by changes in the wind-stress forcing and changes in water mass properties that determine the density contrast between the NS and the Atlantic. Annual mean time series (not shown) of the total (i.e. vertically integrated) transport anomalies from the east (IFR, FS, SN) and from the west (DS) of Iceland are almost perfectly anticorrelated ($r = -0.93$), indicating the importance of the wind-driven barotropic transports that has been described by Biastoch et al. (2003). Variations of the dense outflows through DS are very similar to the total DS transport changes and both time series are correlated with $r = 0.8$. In contrast, the dense FS outflow does not show that high correlation with the total flow, regardless of taking the boundary at 27.6 or 27.8. Therefore, the FS and DS overflow do not show the clear anticorrelated behaviour that was reported by Köhl et al. (2007).

For hydraulic control, Whitehead's formula (Eq. 22.1) predicts an upper limit of the overflow transports that is proportional to the density contrast and the square of the upstream reservoir height above the sill. In the presence of rotation and friction, smaller values of the transports are expected, but outflow variations will depend on reservoir height and density changes, where the former (due to the quadratic term) is probably more important, as discussed by Macrander et al. (2005). They were able to reconstruct the observed transports from variations of the 27.8 interface at the Kögur section. In the simulations, we find indeed high correlations ($r > 0.8$) between the transports and the interface variations near the entrance of the Denmark Strait (Fig. 22.7a). Correlations are also relatively high in the Iceland Sea and along the GSR. At lag 0 years, there are also regions with significantly high negative correlation (indicating relatively deep interface depth) in the Norwegian Sea, a finding that is further discussed below. Using (Eq. 22.1) and a density contrast of 0.39 kg m^{-3}, we are able to reconstruct (Fig. 22.8a) the transport changes from the variations of the $\sigma = 27.8$ interface depths taken from an average over 4 grid points entered near 67° N, 24° W (see Fig. 22.7a). For the FS outflow, we find significant correlations only for a few grid cells just upstream of the FS section (Fig. 22.7b). Using interface variations from that point, however, enables one to reconstruct also the FS outflow (Fig. 22.8b). Hansen et al. (2001) have tried to reproduce FBC outflow variation in the second half of the 20th century by relating them to the interface variations far upstream at weather ship Mike. Even though our results may be influenced by the relatively coarse resolution in FS, the findings support Helfrich and Pratt's (2003) conclusion that a strong relation between the outflow and the interface depth exists only close to the entrance of the outflow channel.

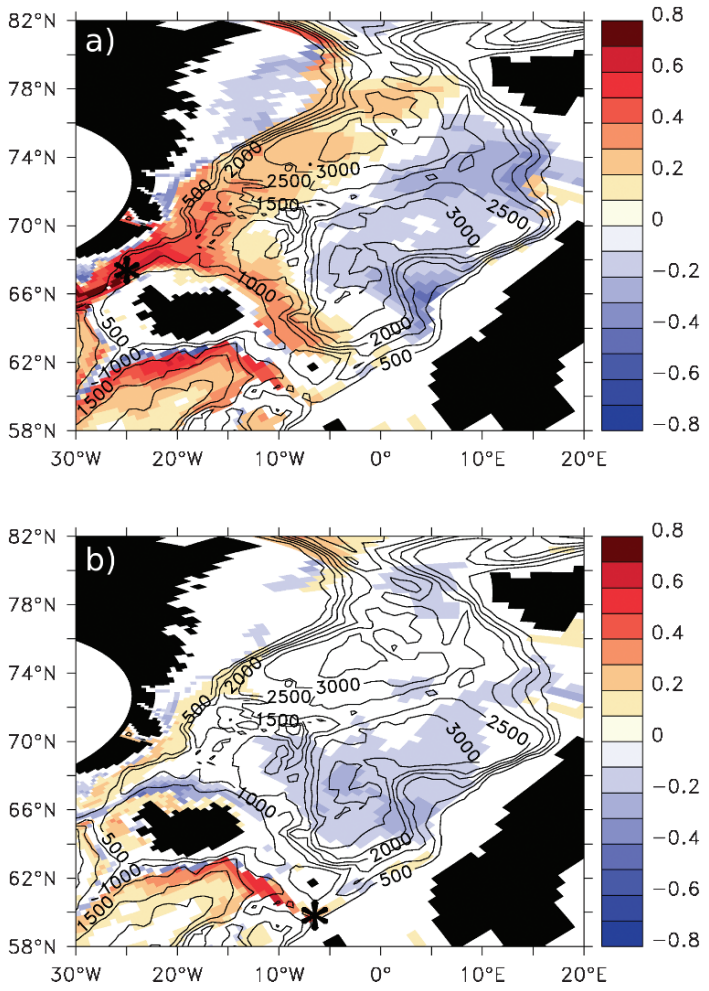

Fig. 22.7 Correlation coefficients between the depth of the 27.8 isopycnal and (**a**) the DS outflow, and (**b**) the FS outflow at zero lag. Positive correlations indicate negative depth (positive thickness) anomalies at enhanced (negative) outflow transports. A * symbol indicates the location where time series of the interface height were taken to reconstruct the respective outflow transports

Köhl et al. (2007) were able to reconstruct the modelled overflow transport from modelled SSH variations in DS. The correlation map from the 505-year annual mean time series from the coupled experiment (Fig. 22.9a) bears remarkable resemblance to the monthly data from Köhl et al.'s high-resolution regional model (Fig. 22.9b). Correlations are high around Iceland (indicating the enhancement of the circulation around the island). In the coupled climate model the correlations between the SSH and the DS overflow time series exceed 0.7 and allow for a reconstruction of the deep transports (Fig. 22.8a) from the regression, explaining more than 50% of the

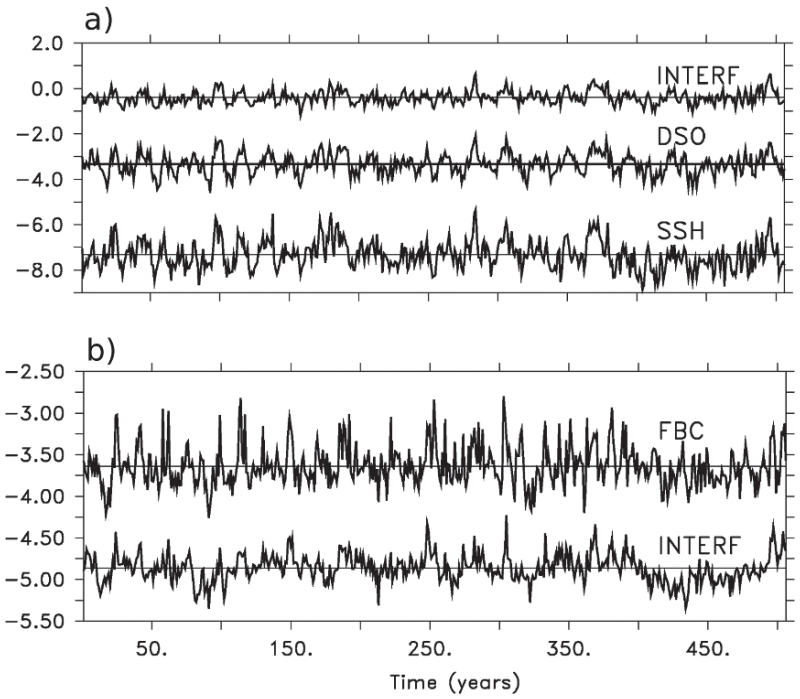

Fig. 22.8 Time series (annual means) of (**a**) simulated Denmark Strait overflow ($\sigma > 27.8$, DSO) and (**b**) Faroe Bank Channel overflow ($\sigma > 27.6$, FBC). Units are Sv, negative sign indicates flow out of the NS. Also included are reconstructed transports from the hydraulic relation (1) (INTERF) and, for DS also from the sea surface height (SSH) variations. Offsets for the DS reconstructions are +4 Sv and −4 Sv, respectively and for the FBC reconstruction −1.5 Sv. Correlations between the DSO and the SSH and the interface reconstructions are 0.73 and 0.8, respectively. Correlation between FBC and the interface reconstruction is 0.67

overflow's variance. For the FBC outflow, however, we do not find the expected relation of interface and surface elevation (i.e. a depression of SSH at times of strong outflow). Correlations are negative all over the northwest European Continental Slope (not shown). One might think that this is related to the coarse resolution of the throughflow channel in the coupled model. However, the respective data from the high-resolution model (kindly provided by A. Köhl) also gives only low correlation (albeit of various sign) over the FBC.

The total flow through DS is correlated (not shown) to the NAO with $r = -0.43$ and the total flow through the Iceland–Scotland section is similarly correlated with a reversed sign. A running correlation indicates that the relation between the NAO and the GSR exchange flows varies with time, indicating shifting atmospheric pressure patterns likely similar to the ones observed in the second half of the 20th century (Jung et al. 2003). The DS overflow is correlated to the NAO with $r = -0.32$ (correlations $r > 0.2$ are considered significant) at zero lag (Fig. 22.10). The lagged

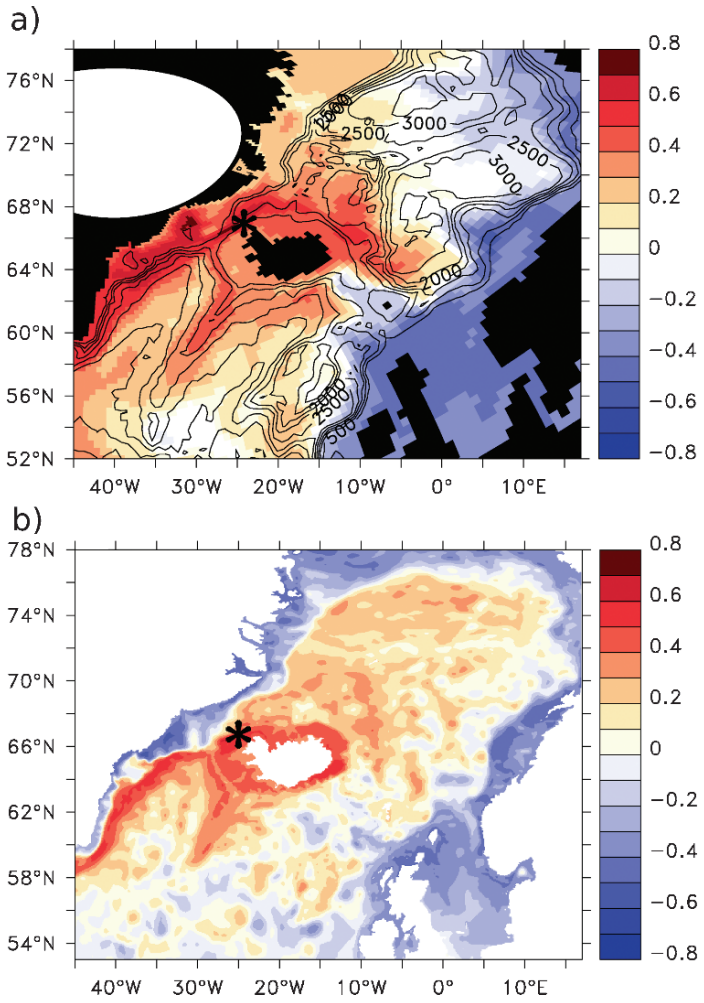

Fig. 22.9 Correlation (at zero lag) coefficients between the Denmark Strait overflow and the sea surface elevation (SSH) derived from (**a**) the coupled ECHAM5/MPIOM, and (**b**) from a high resolution regional model (redrawn after Köhl et al. 2007). The outflow has negative sign so that positive correlations mean depression of the sea surface. A * symbol indicates the location where SSH time series were taken to reconstruct the respective outflow transports

correlations show some asymmetry around zero, which might indicate a certain response to the (white noise) NAO forcing. The NAO may affect the overflows in several ways. First, there is the barotropic response to changes in the wind stress. Second, the heat flux pattern associated with a negative NAO index favours convection in the Greenland and Iceland Sea (Dickson et al. 2000) and the increase

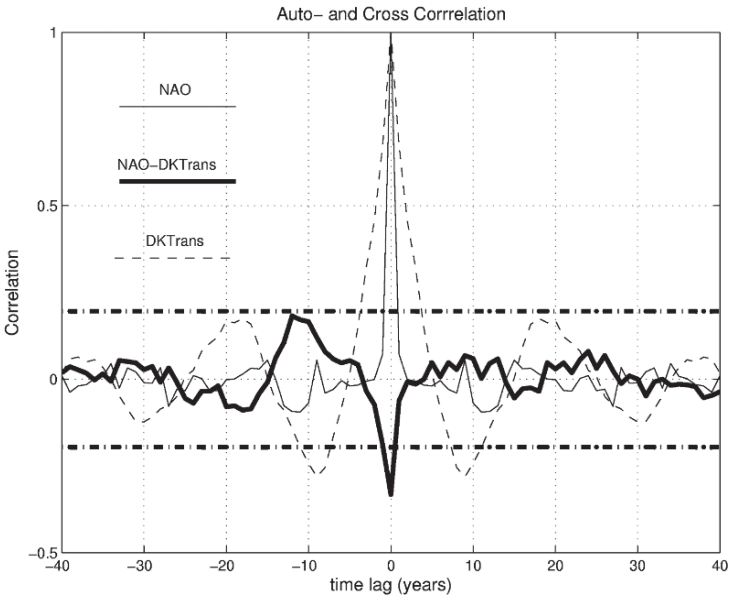

Fig. 22.10 (Lag) correlation coefficients between the annual mean NAO and (solid thick line) the dense overflow transport through DS. Note that overflows (outflows) are defined with a negative sign so that high positive NAO is associated with high overflow transports. Negative time lags indicate NAO leading. Thick dashed lines indicate the 99% confidence interval. Also included are the autocorrelation functions for the DS overflow (thin dashed line) and for the NAO (thin solid line)

in reservoir height would lead to more outflow. Third, the inflow of Atlantic waters also depends on the NAO. Given that the overflows consist of more or less of Atlantic Water, the changing conditions at the entrance may be traced, with a time lag of a few years, to the overflows (Dickson et al. 1999). While the first mechanism is fast and barotropic, the latter two will require some time lag for the anomalies to reach DS and may integrate the high-frequency forcing variability in time. Spectra of the overflow time series (not shown) indicate elevated energy in the interdecadal band with a peak at 20 years. A detailed investigation of the multidecadal variability is beyond the scope of this paper. One explanation, as to how a white-noise (NAO) forcing can generate a red-noise response has been given by Käse (2006): A controlled volume box model, where accumulation in volume is driven by net imbalances between prescribed inflow, outflow, and NAO-derived flux through the interface, results in a Riccati equation for filling and flushing. For small interface fluctuations with white-noise forcing, the overflow spectrum is red-noise with a timescale between 5 and 15 years. The proposed mechanism is an effective low-pass filter for higher frequency variations and the long-term changes in the DS transports are a reflection of coupled ocean–atmosphere interactions. There are several limitations in the simple model but comparisons to observations indicate that such a concept

can be useful when a strongly limiting process such as hydraulic control dominates the outflow. However, further investigations using long integrations with models resolving the important processes are necessary to better understand the mechanisms behind the low-frequency variations in the overflows.

22.7 Summary and Conclusion

Various aspects of the representation of the overflows in state-of-the-art models have been reviewed. At high-enough resolution, numerical models are able to reproduce the structure and dynamics of the overflows. The representation of the overflows in coarse-resolution ocean models has been improved but is far from being perfect. In the ECHAM5/MIOM simulation analysed here, main shortcomings can be seen in the water mass properties of the overflows and the downslope evolution of the plume south of the GSR. On the other hand, the model reproduces the current structure and the hydraulic character of the overflows remarkably well. The model results confirm previous findings that there is a strong coupling between the dense overflow in the DS and the SSH variations above. This suggests that DS transport variations can be monitored by satellite altimetry. However, a first attempt by Köhl et al. (2007) revealed unforeseen difficulties. In order to be able to monitor small long-term transport changes from altimeter, very high accuracy is required.

The coupled ocean–atmosphere model is able to reproduce a realistic 6 Sv of overturning across the GSR, whereas many previous climate models closed their overturning cell by convection to the south of the GSR. This has consequences for the stability of the THC in climate change simulations, which, for the IPCC AR4, are presently being assessed. Results from the MPI-M model and from the NCAR model (Hu et al. 2004; Jungclaus et al. 2006b) show that there is a considerable decrease, but no breakdown of the THC in the greenhouse gas induced warmer climate. In contrast to the maximum of the overturning streamfunction, however, the overflow transports increase slightly in both models even though the water mass properties to the north and to the south of the GSR change dramatically. Hence, the reduction of the overturning takes place only to the south of the GSR, where open ocean convection in the Labrador Sea forms a more direct and apparently more vulnerable component of the THC. In contrast, the hydraulic system of the overflows keeps working and this stabilizes the THC. According to these studies, the overflows across the GSR provide the backbone of a substantial overturning circulation even in a warmer climate.

Acknowledgements Funding for this study was (in part) provided by the Deutsche Forschungsgemeinschaft Special Research Grants (SFB 460: IfM-Geomar Kiel and SFB 512: IfM Hamburg). The ECHAM5/MPIOM model simulations have been carried out at the German Climate Computing Center (DKRZ).

References

Baringer MO, Price, JF (1997) Mixing and spreading of the Mediterranean outflow. J Phys Oceanogr 27: 1654–1677.

Beckmann E, Döscher R (1997) A method for improved representation of dense water spreading over topography in geopotential coordinate models. J Phys Oceanogr 27: 581–591.

Bengtson L, Hodges KI, Roeckner E (2006) Storm tracks and climate change. J Climate, 19: 3518–3543.

Biastoch A, Käse RH, Stammer DB (2003) The sensitivity of the Greenland-Scotland overflow to forcing changes. J Phys Oceanogr 33: 2307–2319.

Blindheim J, Østerhus S (2005) The Nordic Seas, Main oceanographic features. In: Drange H et al. (eds): The Nordic Seas: An integrated perspective, oceanography, climatology, biogeochemistry, and modelling. American Geophysical Union, Geophysical Monograph 158, pp. 11–37.

Borenäs K, Lundberg P (1988) On the deep-water flow through the Faroe Bank Channel. J Geophys Res 93: 1281–1292.

Borenäs K, Lundberg P (2004) The Faroe-Bank Channel deep-water overflow. Deep-Sea Res II 51: 335–350.

Bruce JG (1995) Eddies southwest of Denmark Strait. Deep-Sea Res I 42: 13–29.

Campin J-M, Goosse H (1999) Parameterization of density-driven downslope flow for a coarse-resolution ocean model in z-coordinates. Tellus 51: 412–430.

Dickson RR, Brown J (1994) The production of North Atlantic Deep Water: Sources, rates, and pathways. J Geophys Res 99: 12319–12341.

Dickson RR, Meincke J, Vassie I, Jungclaus J, Østerhus S (1999) Possible predictability in overflow from the Denmark Strait. Nature 397: 243–246.

Dickson RR et al. (2000) The Arctic response to the North Atlantic Oscillation. J Climate 13: 2671–2696.

Drange H, Gerdes R, Gao Y, Karcher M, Kauker F, Bentsen M (2005) Ocean general circulation modelling of the Nordic Seas. In: Drange et al. (eds): The Nordic Seas: An integrated perspective, oceanography, climatology, biogeochemistry, and modelling. American Geophysical Union, Geophysical Monograph 158, pp. 199–219.

Ezer T (2006) Topographic influence on overflow dynamics: Idealized numerical simulations and the Faroe Bank Channel overflow. J Geophys Res 111: C02002, doi:10.1029/2005JC003195.

Gill AE (1977) The hydraulics of rotating channel flow. J Fluid Mech 80: 641–671.

Girton JB, Sanford TB (2003) Descent and modification of the overflow plume in the Denmark Strait. J Phys Oceanogr 33: 1351–1364.

Gulev SK, Barnier B, Knochel H, Molines J-M, Cottet M (2003) Water mass transformation in the North Atlantic and its impact on the meridional circulation: Insights from an ocean model forced by NCEP-NCAR reanalyses surface fluxes. J Climate 16: 3085–3110.

Haak H, Jungclaus JH, Mikolajewicz U, Latif M (2003) Formation and propagation of great salinity anomalies. Geophys Res Lett 30: 1473, doi:10.1029/2003GL017065.

Hallberg R (2000): Time integration of diapycnal diffusion and Richardson-number-dependent mixing in isopycnal coordinate ocean models. Mon Wea Rev 128: 1402–1419.

Hansen B, Turell WR, Østerhus S (2001) Decreasing overflow from the Nordic Seas into the Atlantic Ocean through the Faroe Bank Channel since 1950. Nature 411: 927–930.

Helfrich KR, Pratt L (2003) Rotating hydraulics and upstream basin circulation. J Phys Oceanogr 33: 1651–1663.

Hu A, Meehl GA, Washington WM, Dai A (2004) Response of the Atlantic Thermohaline Circulation to increased atmospheric CO_2 in a coupled model. J Climate 17: 4267–4279.

Jakobsen PK, Ribergaard MH, Quadfasel D, Schmith T, Hughes CW (2003) Near-surface circulation in the northern North Atlantic as inferred from Lagrangian drifters: Variability from the mesoscale to interannual. J Geophys Res 108: 3251, doi:10.1029/2002JC001554.

Jiang L, Garwood RW (1996) Three-dimensional simulations of overflows on the continental slopes. J Phys Oceanogr 26: 1214–1233.

Jónsson S, Valdimarsson H (2004) A new path for the Denmark Strait overflow water from the Iceland Sea to Denmark Strait. Geophys Res Lett 31: L03305, doi:10.1029/2003GL019214.
Jung T, Hillmer M, Ruprecht E, Kleppek S, Gulev SK, Zolina O (2003) Characteristics of the recent eastward shift of interannual NAO variability. J Climate 16: 3371–3382.
Jungclaus JH, Backhaus JO (1994) Application of a transient reduced gravity plume model to the Denmark Strait overflow. J Geophys Res 99: 12375–12396.
Jungclaus JH, Vanicek M (1999) Frictionally modified flow in a deep ocean channel: Application to the Vema Channel. J Geophys Res 104: 21123–21136.
Jungclaus JH, Hauser J, Käse RH (2001) Cyclogenesis in the Denmark Strait overflow plume. J Phys Oceanogr 31: 3214–3229.
Jungclaus JH, Botzet M, Haak H, Keenlyside N, Luo J-J, Latif M, Marotzke J, Mikolajewicz U, Roeckner E (2006a) Ocean circulation and tropical variability in the coupled model ECHAM5/MPI-OM. J Climate 19: 3952–3972.
Jungclaus JH, Haak H, Esch M, Roeckner E, Marotzke J (2006b) Will Greenland melting halt the thermohaline circulation? Geophys Res Lett 33: L17708, doi:10.1029/2006GL026815.
Käse RH, Oschlies A (2000) Flow through Denmark Strait. J Geophys Res 105: 28527–28546.
Käse RH (2006) A Riccati model for the Denmark Strait overflow variability. Geophys Res Lett 33: L21S09, doi:10.1029/2006GL026915.
Killworth PD, McDonald NR (1993) Maximal reduced gravity flux in rotating hydraulics. Geophys Astrophys Fluid Dyn 70: 31–40.
Killworth PD, Edwards NR (1999) A turbulent bottom boundary layer code for use in numerical ocean models. J Phys Oceanogr 29: 1221–1238.
Killworth PD (2001) On the rate of descent of overflows. J Geophys Res 106: 22267–22275.
Köhl A, Käse RH, Stammer D, Serra N (2007) Causes of changes in the Denmark Strait overflow. J Phys Oceanogr 37: 1678–1696.
Kösters F, Käse RH, Schmittner A, Herrmann P (2005) The effect of Denmark Srait overflow on the Atlantic Meridional Overturning Circulation. Geophys Res Lett 32: L04602, doi:10.1029/2004GL022112.
Legg S, Hallberg RW, Girton JB (2006) Comparison of entrainment in overflows simulated by z-coordinate, isopycnal and non-hydrostatic models. Ocean Modelling 11: 69–97.
Macdonald AM (1998) The global ocean circulation: a hydrographic estimate and regional analysis. Prog Oceanogr 41: 281–382.
Macrander A (2004) Variability and processes of the Denmark Strait overflow. Ph.D. thesis. IfM Geomar, Leibniz Institut für Meereswissenschaften an der Universität Kiel, 177 pp.
Macrander A, Send U, Valdimarsson H, Jónsson S, Käse RH (2005) Interannual changes in the overflow from the Nordic Seas into the Atlantic Ocean through Denmark Strait. Geophys Res Lett 32: L06606, doi:10.1029/2004GL021463.
Marsland SJ, Haak H, Jungclaus JH, Latif M, Röske F (2003) The Max- Planck- Institute global ocean/sea ice model with orthogonal curvilinear coordinates. Ocean Modelling 5: 91–127.
Müller WA, Roeckner E (2006) ENSO Impact on Mid-Latitude Circulation Patterns in Future Climate Change Projections. Geophys Res Lett 33: L05711, doi: 10.1029/2005GL025032.
Nikolopoulos AN, Borenäs K, Hietala R, Lundberg P (2003) Hydraulic estimates of the Denmark Strait overflow. J Geophys Res 108: 3095, doi:10.1029/2001JC001283.
Nilsen JEØ, Gao Y, Drange H, Furevik T, Bentsen M (2003) Simulated North Atlantic-Nordic Seas water mass exchange in an isopycnic coordinate OGCM. Geophys Res Lett 30: 1536, doi:10.1029/2002GL016597.
Østerhus S, Turrell WR, Jónsson S, Hansen B (2005) Measured volume, heat, and salt fluxes from the Atlantic to the Arctic Mediterranean. Geophys Res Lett 32: L07603, doi:10.1029/2004GL022188.
Özgökmem TM, Fischer PF, Johns WE (2006) Product water mass formation by turbulent density currents from a high-order nonhydrostatic spectral element model. Ocean Modelling 12: 237–267.
Pratt LJ, Smeed DA (2004) The physical oceanography of sea straits (Editorial). Deep-Sea Res II 51(4–5): 319.

Price JF, Baringer MO (1994) Outflow and deep water production by marginal seas. Progr Oceanogr 33: 161–200.
Riemenschneider U, Legg S (2007) Regional simulations of the Faroe Bank channel overflow in a level model. Ocean Modelling 17: 93–122.
Roberts MJ, Wood RA (1997) Topography sensitivity studies with a Bryan-Cox type ocean model. J Phys Oceanogr 27: 823–836.
Ross CK (1984) Temperature-salinity characteristics of the "overflow" water in Denmark Strait during "Overflow '73". Rapp P-v Reun Cons Int Explor Mer 185: 111–119.
Roeckner E, Bäuml G, Bonaventura L, Brokopf R, Esch M, Giorgetta M, Hagemann S, Kirchner I, Kornblueh L, Manzini E, Rhodin A, Schlese U, Schulzweida U, Tompkins A (2003) The atmospheric general circulation model ECHAM5, part I: Model description. Max- Planck-Institut für Meteorologie, Report No. 349, 127 pp.
Saunders P (1990) Cold outflow from the Faroe Bank Channel. J Phys Oceanogr 20: 29–43.
Schmittner A, Latif M, Schneider B (2005) Model projections of the North Atlantic thermohaline circulation for the 21st century assessed by observations. Geophys Res Lett 32: L23710, doi:10.1029/GL024368.
Schweckendiek U, Willebrand J (2005) Mechanisms affecting the overturning response in global warming simulations. J Climate 18: 4925–4936.
Shi XB, Roed LP, Hackett B (2001) Variability of the Denmark Strait overflow: A numerical study. J Geophys Res 106: 22277–22294.
Smith PC (1975) A stream-tube model for bottom boundary currents in the ocean. Deep-Sea Res 22: 853–873.
Song Y, Chao Y (2000) An embedded bottom boundary layer formulation for z-coordinate models. J Ocean Atmos Tech 17: 546–560.
Stammer D, Wunsch C, Fukumori I, Marshall J (2002) State estimation improves prospects for ocean research. EOS Transactions 83: 294–295.
Steele M, Morley R, Ermold W (2001) PHC: A global ocean hydrography with high-quality Arctic Ocean. J Climate 14: 2079–2087.
Stern ME (2004) Transport extremum through Denmark Strait. Geophys Res Lett 31: L12303, doi:10.1029/2004GL020184.
Stocker TF et al. (2001) Physical climate processes and feedbacks. In: Climate Change 2001: The scientific basis, Intergovernmental Panel of Climate Change (IPCC) Technical summary of the Working Group 1 Report, Cambridge University Press, New York, pp. 418–470.
Whitehead JA (1989) Internal hydraulic control in rotating fluids: Application to oceans. Geophys. Astrophys Fluid Dyn 36: 187–205.
Whitehead JA (1998) Topographic control of oceanic flows in deep passages and straits. Rev Geophys 36: 423–440.
Willebrand J et al. (2001) Circulation characteristics in three eddy-permitting models of the North Atlantic. Progr Oceanogr 48: 123–161.
Winton M, Hallberg RW, Gnanadesikan A (1998) Simulation of density-driven frictional downslope flow in z-coordinate ocean models. J Phys Oceanogr 28: 2163–2174
Xu X, Chang YS, Peters H, Özgökmem TM, Chassignet EP (2006) Parameterization of gravity current entrainment for ocean circulation models using a high-order 3d nonhydrostatic spectral element model. Ocean Modelling 14: 19–44.
Zhang J, Steele M, Rothrock DA, Lindsay RW (2004) Increasing exchanges at Greenland-Scotland Ridge and their links with the North Atlantic Oscillation and Arctic sea ice. Geophys Res Lett 31: L09307, doi:10.1029/2003GL019304.